



Characteristics and properties of a novel in situ method of synthesizing mesoporous TiO₂ nanopowders by a simple coprecipitation process without adding surfactant



Shang-Wei Yeh^{a,b}, Horng-Huey Ko^a, Hsiu-Mei Chiang^c, Yen-Ling Chen^{a,*}, Jian-Hong Lee^d, Chiu-Ming Wen^b, Moo-Chin Wang^{a,**}

^a Department of Fragrance and Cosmetic Science, Kaohsiung Medical University, 100 Shih-Chuan 1st Road, Kaohsiung 80782, Taiwan

^b Department of Life Science, National University of Kaohsiung, 700 Kaohsiung University Road, Kaohsiung 811, Taiwan

^c Department of Cosmeceutics, China Medical University, 91 Hsueh-Shih Road, Taichung 40402, Taiwan

^d Clean Energy and Eco-Technology Center, Industrial Technology Research Institute, 8 Gongyan Road, Tainan 734, Taiwan

ARTICLE INFO

Article history:

Received 23 March 2014

Accepted 31 May 2014

Available online 11 June 2014

Keywords:

Mesoporous TiO₂ nanopowders

In situ synthesis

Coprecipitation process

Anatase

Rutile

ABSTRACT

In situ synthesis of mesoporous TiO₂ nanopowders using titanium tetrachloride (TiCl₄) and NH₄OH as initial materials has been successfully fabricated by a coprecipitation process without the addition of surfactant. Characteristics and properties of the mesoporous TiO₂ nanopowders were investigated using differential scanning calorimetry/thermogravimetry (DSC/TG), X-ray diffraction (XRD), Brunauer–Emmett–Teller (BET) and Barrent–Joyner–Halenda (BJH) analyses, transmission electron microscopy (TEM), selected area electron diffraction (SAED) and high resolution TEM (HRTEM). The results of TG and XRD showed that the NH₄Cl decomposed between 513 and 673 K. XRD results showed that the anatase TiO₂ only contained a single phase when the calcination temperature of the precursor powder was less than 673 K. Whereas phases of anatase and rutile TiO₂ coexist after calcining at 773 K for 2 h. The crystalline size of the anatase and rutile TiO₂ was 14.3 and 26.6 nm, respectively, when the precursor powder was calcined at 773 K for 2 h. The BET and BJH results showed a significant increase in surface area and pore volumes when the NH₄Cl was completely decomposed. The maximum values of BET specific surface area and volume were 172.8 m²/g and 0.392 cm³/g, respectively. The average pore sizes when calcination was at 473 and 773 K for 2 h were 3.8 and 14.0 nm, respectively.

© 2014 Elsevier B.V. All rights reserved.

1. Introduction

Ultraviolet A (UVA, 320–400 nm) is a major culprit in photoaging and causing skin cancers. Even UVB (280–320 nm) radiation, which primarily reaches the top-most layer of the skin, is responsible for acute photodamage including sunburn and some non-melanoma skin cancers [1]. Therefore, protecting humans against UVA and UVB radiation is a matter of great important. Certain minerals can be used as sun-attenuating or sunscreen agents for protection against the adverse effects of UVA and UVB radiation. Titanium dioxide (TiO₂) is an important powder frequently used in sunscreens as an inorganic physical sun blocker due to its being more effective in the UVB region [2]. But micron-sized TiO₂

powders create an opaque layer in the skin. To solve the cosmetic drawback of TiO₂ opaque sunscreen, micron-sized TiO₂ particles must be replaced by TiO₂ nanoparticles.

The use of TiO₂ in cosmetics as a sunscreen agent requires high purity with controlled crystalline size, surface properties, definite phase content and morphology. The metastable anatase and stable rutile phases are the two most important polymorphs of TiO₂ [3]. These polymorphs exhibit various properties and, consequently, different sunscreen performances.

Recently, several techniques such sol–gel [4,5], non-hydrolytic sol–gel [6], hydrothermal [7,8] and coprecipitation [9–11] processes have been widely used to prepare nanosized TiO₂ powders in a way that offers great control over their properties such as crystalline phase, crystallite size and morphology and surface area. Moreover, mesoporous TiO₂ prepared using the sol–gel route was first reported by Antonelli and Ying [12]. These mesoporous TiO₂ powders are of particular interest because their channels offer a large surface area and their pore wall framework is nanocrystalline. On the other hand,

* Corresponding author. Tel.: +886 7 3121101x2584; fax: +886 7 3210683.

** Corresponding author. Tel.: +886 7 3121101x2366; fax: +886 7 3210683.

E-mail addresses: yelichen@kmu.edu.tw (Y.-L. Chen), mchwang@kmu.edu.tw (M.-C. Wang).

the thermal stability of mesoporous TiO₂ is greater than that of traditional TiO₂ nanoparticles [13].

In recent years, mesoporous TiO₂ nanoparticles possessing various pore size distributions have been successfully fabricated using diblock copolymers via a sol–gel process in aqueous solution, as reported by Kim et al. [14]. They demonstrated that their mesoporous TiO₂ nanoparticles could have multiple specific surface areas of 186, 210 or 192 m²/g with average pore sizes of 5.1, 6.1 and 6.4 nm, respectively depending on the type of diblock copolymer, and crystallite sizes of 8.1, 8.3 and 8.8 nm when the precursor powder was first calcined at 673 K. Hung et al. [13] synthesized ordered hexagonal mesoporous TiO₂ nanoparticles using an evaporation-induced self-assembly (EISA) route with Pluronic P123 and tetrabutyl orthotitanate (Ti(OBU)₄) as the templating agent respectively. Further, Herregods et al. [15] also reported that mesoporous TiO₂ nanosized powders with a controlled uniform pore size could be synthesized by the EISA route used the diblock copolymer Brij 58 as surfactant. They indicated that the pore structure of a mesostructured TiO₂ nanopowder was dependent on the thermal stabilization and template removal. In addition, various surfactants such as cetyl-trimethyl ammonium bromide (CTAB), cetyl-trimethylammonium chloride (CTAC), benzalkonium chloride (BC) or octadecyl-trimethyl ammonium bromide (C₁₈TAB) could assist the sol–gel reaction at different calcination temperatures and affect the formation of mesoporous TiO₂ nanocrystalline powders, as also pointed out by Casino et al. [16].

As mentioned above, mesoporous TiO₂ nanosized powders are usually synthesized using a surfactant. The synthesis of mesoporous TiO₂ nanopowders without a surfactant added has not been discussed in detail. Therefore, in the present study we attempted to use residual ammonium chloride (NH₄Cl) as the agent of pore formation for in situ synthesis of mesoporous TiO₂ nanosized powders prepared by a simple coprecipitation process. The characteristics and properties of the mesoporous TiO₂ nanopowders were investigated by calorimetry/thermogravimetry (DSC/TG), X-ray diffraction (XRD), Brunauer–Emmett–Teller (BET) and Barrent–Joyner–Halenda (BJH) analyses, transmission electron microscopy (TEM), selected area electron diffraction (SAED) and high resolution TEM (HRTEM).

The scope of this work is focused on: (i) studying the thermal behavior of the TiO₂ precursor powder with residual NH₄Cl, (ii) determining the phase transition of the TiO₂ precursor powder with NH₄Cl after calcination, (iii) evaluating the surface areas and pore sizes of the mesoporous TiO₂ nanopowders and (iv) observing the microstructures of the mesoporous TiO₂ nanopowders by TEM.

2. Experimental procedure

2.1. Sample preparation

The TiO₂ precursor powder with residual NH₄Cl was prepared using a simple coprecipitation route. The initial materials included titanium tetrachloride (TiCl₄, purity ~98.5%, supplied by Nihon Shiyaku Reagent, Japan) and aqueous NH₄OH solution (purity ~28%, supplied by Nihon Shiyaku Reagent, Japan). TiCl₄ was dissolved in deionized water with a volume ratio of 1:20 and the mixed solution was stirred using a magnetic stirrer and heated to 348 K for 2 h. Under these conditions Ti⁴⁺ formed, but due to the very low pH value of the Ti⁴⁺ solution, no precipitation occurred. In order to increase the pH and promote precipitation, aqueous NH₄OH solution must be added to the mixture as a precipitating agent. When the NH₄OH was slowly added to the water–TiCl₄ mixture until the pH adjusted to 7, then precipitation took place. Subsequently, the precipitates were freeze dried at 218 K in a vacuum without washing.

2.2. Sample characterization

Differential scanning calorimetry/thermogravimetry (DSC/TG, SDT Q600, TA) analysis was conducted on 200 mg of TiO₂ precursor powder at a heating rate of 10 K/min in static air up to 1173 K. Al₂O₃ powder was used as the reference material.

The crystalline phases of the TiO₂ precursor powder after calcining at various temperatures for 2 h were identified by X-ray diffraction (XRD, Model Rad IIA, Rigaku, Tokyo) with Cu K α radiation and an Ni filter, operating at 40 kV, 30 mA and a scanning rate (2 θ) of 1°/min. The crystallite sizes (*D*) of the anatase and rutile TiO₂ were calculated using Scherrer's equation [17].

$$D = 0.9\lambda / (\beta \cos \theta) \quad (1)$$

where $\lambda = 1.5405 \text{ \AA}$ is the wavelength of the Cu K α radiation, and β is the full-width at half-maximum (FWHM) intensity in radians. The (101) and (110) reflections at $2\theta = 25.32^\circ$ and 27.48° were used to define the FWHM intensity of anatase and rutile TiO₂, respectively, within their various crystalline phases, and θ is the Bragg's angle.

Spurr and Myers [18] have also used reflection intensities in the XRD pattern to determine the anatase TiO₂ content. The integrated intensity ratio of the anatase TiO₂ content was defined as follows:

$$f_A = \frac{I_A}{1.265I_R + I_A} \quad (2)$$

where f_A is the fraction of anatase TiO₂, and I_R and I_A are the intensities of the (101) and (110) reflections for the rutile and anatase TiO₂, respectively.

The surface areas, pore volumes and average pore sizes of the calcined powders were obtained by the conventional nitrogen absorption of the Brunauer–Emmett–Teller (BET) and Barrent–Joyner–Halenda (BJH) analysis methods (Gemini 2360, Micromeritics, USA).

After the TiO₂ precursor powder was calcined at various temperatures for 2 h, the morphology of the product powder was examined by transmission electron microscopy (TEM, JEM-2100F, JEOL, Japan) operated at 200 kV. Each TEM sample was prepared by dispersing the product powder in an ultrasonic bath and then collecting it on a copper grid. Selected area electron diffraction (SAED) was utilized to confirm the phases of the calcined TiO₂ nanocrystallite powder. A high resolution TEM (HRTEM) examination was also performed on the product powder samples.

3. Results and discussion

3.1. Thermal behavior of TiO₂ precursor powder with residual NH₄Cl

Fig. 1 shows the DSC/TG curves of the TiO₂ precursor powder with residual NH₄Cl heated in air at a rate of 10 K/min from 303 K to 1173 K. The TG curve reveals the weight loss in the TiO₂ precursor powder with residual NH₄Cl occurring in a temperature range between room temperature and 860 K, and shows that the weight loss approached an exponential decay from 366 to 721 K. The TG curve of weight loss can be divided into three stages: (i) from room temperature to 366 K, (ii) from 366 to 721 K and (iii) from 721 to 860 K. The weight was maintained as nearly constant when the heating temperature was higher than 860 K.

In the first stage, a weight loss of about 4.1% was attributed to the free water of the physisorbed [19]. In the second stage, about 37.4% of the sample weight was lost. This result was due to deoxygenation and NH₄Cl decomposing from the TiO₂ precursor powder.

When the TiO₂ was synthesized using TiCl₄ as an initial material prepared by a coprecipitation process, then the precipitates were

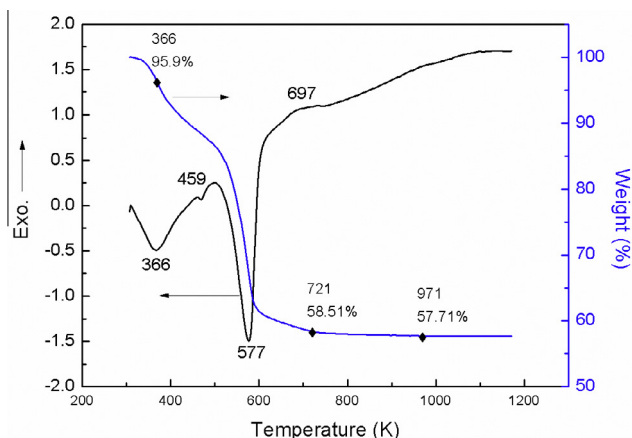


Fig. 1. The DSC/TG curves of TiO₂ precursor powder with residual NH₄Cl content heated at a rate of 10 K/min in static air from 303 K to 1173 K.

washed five times with a large amount of deionized water. The TG curve of this precursor powder had a main weight loss of 17.9%, expressed in the following reaction as reported by Yeh et al. [10].



In the present study, the TiO_2 precipitate was without washing and directly freeze dried; therefore, the precursor powder with residual NH_4Cl content. The precursor obtained in the present study also used TiCl_4 as the initial material and was prepared by the same route as in Yeh et al. [10]. It can be assumed that the reactions in Eq. (3) also hold true in the present study. Therefore, the TiO_2 precursor powder contained about 19.5% residual NH_4Cl .

The third stage of weight loss, about 0.8%, can be assigned to dehydration of surface water molecules most likely existing as a wide set of energetically nonequivalent surface hydrogen groups [20]. In the present work the hydrolysis of the TiCl_4 occurred at low pH. The first step in the hydrolysis caused formation of the $[\text{Ti}(\text{OH})(\text{OH}_2)_5]^{3+}$ species, which was stable under very low pH. Condensation of these species was not able to occur because of the positive charge on the hydroxyl group [21]. When the activity of the solution was high enough to promote deprotonation, $[\text{Ti}(\text{OH})_3(\text{OH}_2)_3]^{+}$ formation led to the condensation of both the anatase and rutile phases, depending on the exact pH [21]. During the deoxygenation taking place at high pH, condensation can proceed along the apical direction, causing formation of the skewed chains of the anatase structure [22,23].

Moreover, the DSC curve also shows that one endothermic peak at 366 K was due to dehydration from the surface of the precursor powder. In addition, one small endothermic peak at 459 K was attributed to partial type I NH_4Cl decomposition (according to Fig. 2). One larger endothermic peak at 577 K was due to complete type I NH_4Cl decomposition. On the other hand, the first broad exothermic peak at 697 K represents the phase transformation from anatase to rutile TiO_2 .

3.2. The phase transition of the TiO_2 precursor powder with residual NH_4Cl after calcination

Fig. 2 shows the XRD patterns of the TiO_2 precursor powder with residual NH_4Cl content after calcining at various temperatures for 2 h. The XRD pattern of the precursor powder before calcination is shown in Fig. 2(a). It reveals the presence of type I NH_4Cl in the precursor powder by the appearance of reflection

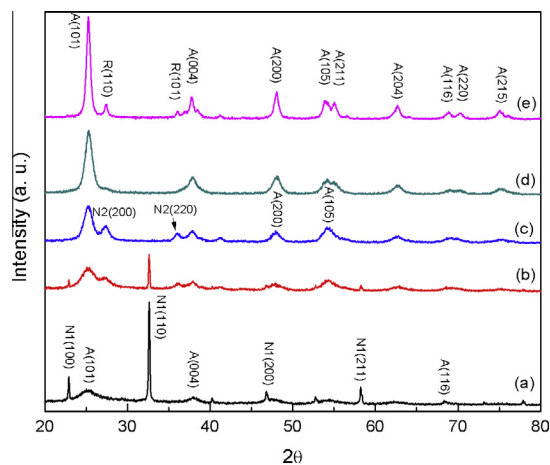


Fig. 2. XRD patterns of TiO_2 precursor powder with residual NH_4Cl content was calcining at various temperatures for 2 h: (a) before, (b) 473 K, (c) 573 K, (d) 673 K and (e) 773 K. ("N1" denotes type I NH_4Cl , "N2" denotes type II NH_4Cl , "A" denotes anatase TiO_2 and "R" denotes rutile TiO_2).

peaks at (100), (110), (200) and (211) (JCPDS Card No. 77-2352). It can also be seen that reflection peaks of (101), (004) and (116) appeared in the anatase TiO_2 (JCPDS Card No. 89-4921). This phenomenon is attributed to crystallines of type I NH_4Cl and anatase TiO_2 coexisting in the precursor powder. However, the crystallinity of anatase TiO_2 was very weak.

Fig. 2(b) shows the TiO_2 precursor powder with residual NH_4Cl content after calcining at 473 K for 2 h. It can be seen that (200) and (105) reflection peaks of anatase TiO_2 initially appear. The (100), (110), (200) and (211) reflection peak intensities of type I NH_4Cl rapidly decrease. However, type II NH_4Cl reflection peaks at (200) and (220) also first appear (JCPDS Card No. 89-2787). This result indicates that the phase transition from type I NH_4Cl into type II NH_4Cl occurred at 437 K.

The XRD pattern of the TiO_2 precursor powder after calcining at 573 K for 2 h is shown in Fig. 2(c), revealing that the anatase TiO_2 becomes the major phase and the type I NH_4Cl has been fully transformed to type II NH_4Cl as the second phase. In addition, the weak intensity and broad appearance of the anatase TiO_2 reflection peaks reveal its poor crystallinity and/or a composition of finer crystallites in the range from the nanometer to the submicron scales [24,25]. Fig. 2(d) shows the XRD pattern of the TiO_2 precursor powder after calcining at 673 K for 2 h, which reveals that the reflection peaks of type II NH_4Cl have disappeared was due to the complete decomposition of type II NH_4Cl . Moreover, the calcined powder only contained a single phase of anatase TiO_2 and the intensities of all the reflection peaks were greater in that anatase in Fig. 2(c). This result occurred because the crystallinity improved and the crystallite size increased as the calcination temperature increased.

Fig. 2(e) shows the precursor powder after calcining at 773 K for 2 h. It can be seen that the intensities of the anatase TiO_2 reflection peaks are continuously improving and sharpening as the calcination temperature increases. The (110) and (101) rutile reflections also first appear (JCPDS Card No. 89-4920), but their crystallinity is very weak.

The average crystallite sizes and phase content of anatase and rutile TiO_2 in the precursor powder after calcining at various temperatures for 2 h can be calculated using Eqs. (1) and (2). The calculated results are listed in Table 1. It can be seen that the crystallite of anatase TiO_2 was only about 2.4 nm before calcining the precursor powder. The crystallite size of anatase TiO_2 increased slightly to 3.3 nm after calcining at 473 K for 2 h because sufficient energy for anatase TiO_2 crystallites was not available. The crystallite size of anatase TiO_2 increased from 6.5 to 14.3 nm when the calcination temperature increased from 573 to 773 K. On the other hand, the crystallite size of rutile TiO_2 was 26.6 nm when the precursor powder was calcined at 773 K for 2 h. When anatase and rutile TiO_2 coexisted in the powder, the crystallite size of the rutile phase was larger than that of anatase TiO_2 . This result was attributed to a critical nuclei size being achieved in the anatase TiO_2 crystallite during the calcination process [26].

On the other hand, before and after calcining between 473 and 673 K for 2 h the precursor powder only contained a single phase of anatase TiO_2 . The phase contents of anatase and rutile TiO_2 were 80.5% and 19.5%, respectively, when the precursor powder was calcined at 773 K for 2 h.

He et al. [27] reported using a hydrolytic TiCl_4 solution with urea for the synthesis of a TiO_2 precursor powder prepared by a membrane process at pH 8 and 368 K. They pointed out the TiO_2 precursor powder was obtained from TiO_2 hydrates without micro-filtration fractionation, and in the precursor powder obtained after calcining at 773 K for 2 h, the phase contents of anatase and rutile TiO_2 were 55.82% and 44.18%, respectively. In addition, when the TiO_2 precursor powder was obtained from TiO_2 hydrates using permeated 5 μm of cellulose acetate membrane fractionation and the

Table 1

Phase contents and crystalline size of TiO₂ precursor powder with residual NH₄Cl content was calcining at various temperatures for 2 h.

Calcination temperatures (K)	Crystalline size (nm)		Ratio of phase content (%)	
	Anatase	Rutile	Anatase	Rutile
Before calcined	2.4	–	100	0
473	3.3	–	100	0
573	6.5	–	100	0
673	10.5	–	100	0
773	14.3	26.6	80.5	19.5

precursor powder was also calcined at 773 K for 2 h, then the calcination product contained just a single phase of anatase TiO₂. Moreover, Liu et al. [28] also described the hydrolysis of titanium tetraisopropoxide at 343 K in pure water with subsequent drying at 373 K for about 100 h, from which the TiO₂ precursor powder was obtained. The phase content of this powder was a mix of anatase and brookite TiO₂. The difference between the previous studies [27,28] and the present work can therefore be attributed to the various initial materials and different synthesis processes used.

The characteristics of the TiO₂ precursor powder with residual NH₄Cl content after calcining at 573 K for various times are shown in Fig. 3, revealing that the calcination products consist of anatase TiO₂ and type II NH₄Cl. It can also be seen that the intensities of the type II NH₄Cl reflection peaks have not changed significantly. Fig. 3 also shows a broad and low intensity anatase (101) reflection peak. This is because the TiO₂ precursor powder calcination at 573 K could not yield complete crystallization, giving a mixture of amorphous and nanocrystalline titania [26]. Moreover, it can also be seen that the diffraction intensity of the anatase (101) reflection peak increases slightly and becomes sharper with prolonged calcination time. This phenomenon can be attributed to the fact that complete crystallization could not occur with calcination at 573 K, but the crystallinity continued to improve and crystalline growth also occurred as the duration increased.

3.3. The surface areas and pore sizes of TiO₂ precursor powder with residual NH₄Cl content after calcination

The results of the N₂ adsorption/desorption analysis of TiO₂ precursor powder with residual NH₄Cl after calcining at various temperatures for 2 h are shown in Fig. 4. Fig. 4(a) shows the N₂ adsorption/desorption curves of TiO₂ precursor powder after

calcining at 473 K. It can be seen that the increase in the volume of adsorption at a relative pressure of P/P_0 , less than 0.3, can be attributed to monolayer N₂ converge of the surface. Whereas, the increase in the relative pressure of P/P_0 by 0.4–0.8 was due to N₂ filling of the mesopores. The absorbed volume was little changed when the relative pressure of P/P_0 was further increased [13]. Moreover, Fig. 4(a) also reveals classical type IV isotherms with an H2 hysteresis loop, which is related to the mesoporous structure [29]. When the desorption branch occurs to located at a relative pressure of P/P_0 around 0.4 for materials with relatively uniform channel-like pores, then an H2 hysteresis loop is observed [30]. On the other hand, the N₂ adsorption/desorption curves show the

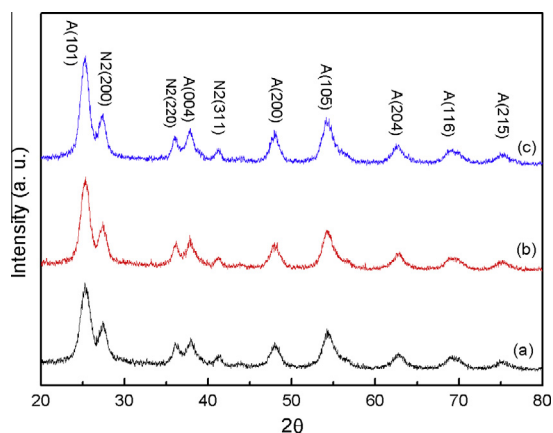


Fig. 3. XRD patterns of TiO₂ precursor powder with residual NH₄Cl content was calcining at 573 K for various times: (a) 10 min, (b) 30 min, and (c) 120 min. ("N2" denotes type II NH₄Cl and "A" denotes anatase TiO₂).

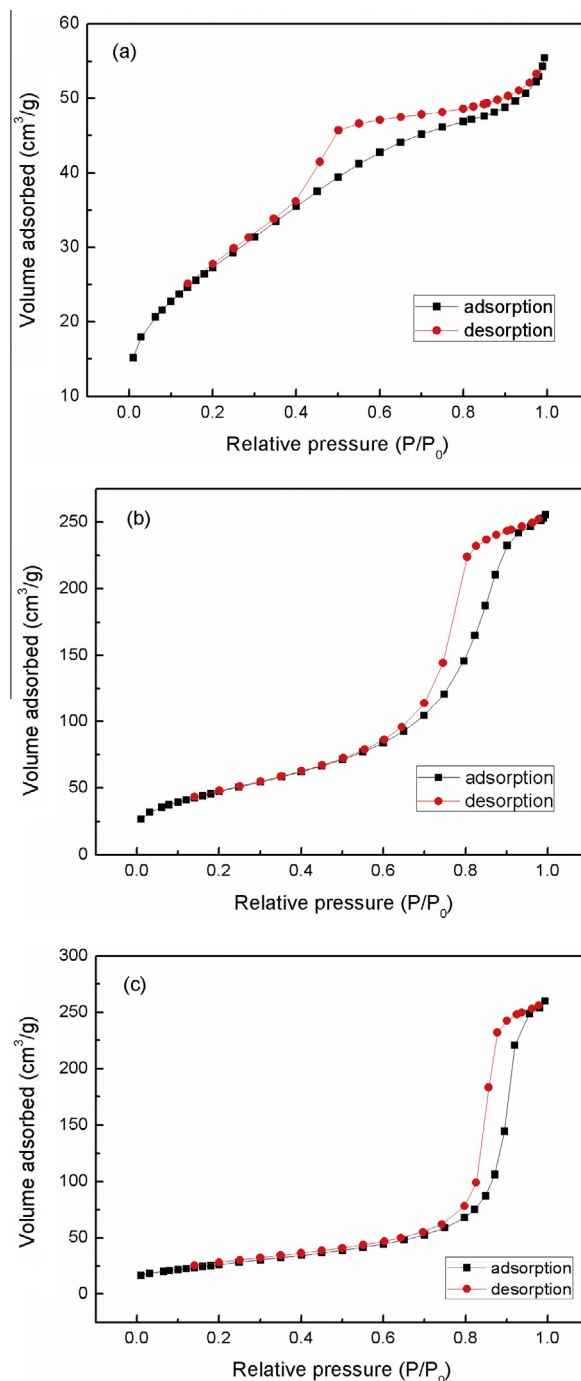


Fig. 4. N₂ adsorption/desorption isotherms curves of TiO₂ precursor powder with residual NH₄Cl content was calcining at various temperatures for 2 h.

Table 2

BET surface area, pore volume and BJH adsorption pore sizes of TiO₂ precursor powder with residual NH₄Cl content was calcining at various temperatures for 2 h.

Calcination temperatures (K)	S_{BET} (m ² /g)	Pore volume (cm ³ /g)	BJH adsorption pore size (nm)
473	99.83	0.081	3.80
573	172.8	0.388	8.00
673	95.8	0.392	14.0

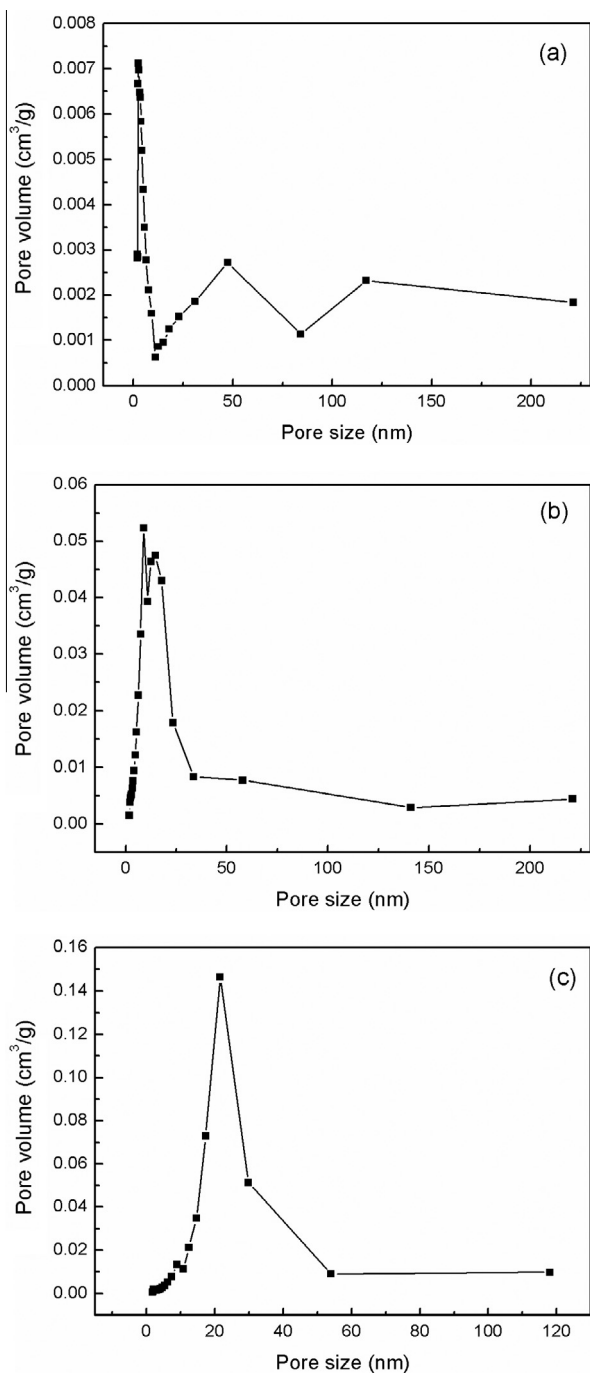


Fig. 5. BJH adsorption pore size distributions of TiO₂ precursor powder with residual NH₄Cl content was calcining at various temperatures for 2 h: (a) 473 K, (b) 573 K and (c) 673 K.

classical type IV with an H2 hysteresis loop, indicating the presence of an ink-bottle-type pore structure with a narrow entrance and a large cavity [14,31].

Fig. 4(b) shows the N₂ adsorption/desorption curves for the TiO₂ precursor powder with residual NH₄Cl content after calcining at 573 K, which also reveals classical type IV isotherms with an H2 hysteresis loop with a relative pressure (P/P_0) range of 0.6–0.9. The relative pressure range of the hysteresis loop for the precursor powder after calcining at 573 K is higher than at 473 K. Kim et al. [14] also reported the hysteresis loop of a given material shifts to a high relative pressure range and steeper when the calcination temperature is increased.

The N₂ adsorption/desorption curves of TiO₂ precursor powder with residual NH₄Cl content after calcining at 673 K are shown in Fig. 4(c). It can be seen that the curves show a classical type IV isotherm with an H1 hysteresis loop in a relative pressure range of 0.75–0.95, which is characteristic of cylindrical pores [13].

The BET surface areas of the TiO₂ precursor powder after calcining at various temperatures for 2 h are listed in Table 1. It can be seen that the surface area was 99.83 m²/g after calcining at 473 K. This value is less than that reported by Kim et al. [14] and Yan et al. [29], but higher than the result of Grujić-Brojčin et al. [4]. The BET surface area increased from 99.83 to 172.8 m²/g when the calcination temperature rose from 473 to 573 K. This value is smaller than the result of Hung et al. [13] but higher than reports in other previous studies [6,15,27,29,32].

It is well known that the BET surface area and pore volume were mainly affected by the growth of the TiO₂ crystallites. However, the

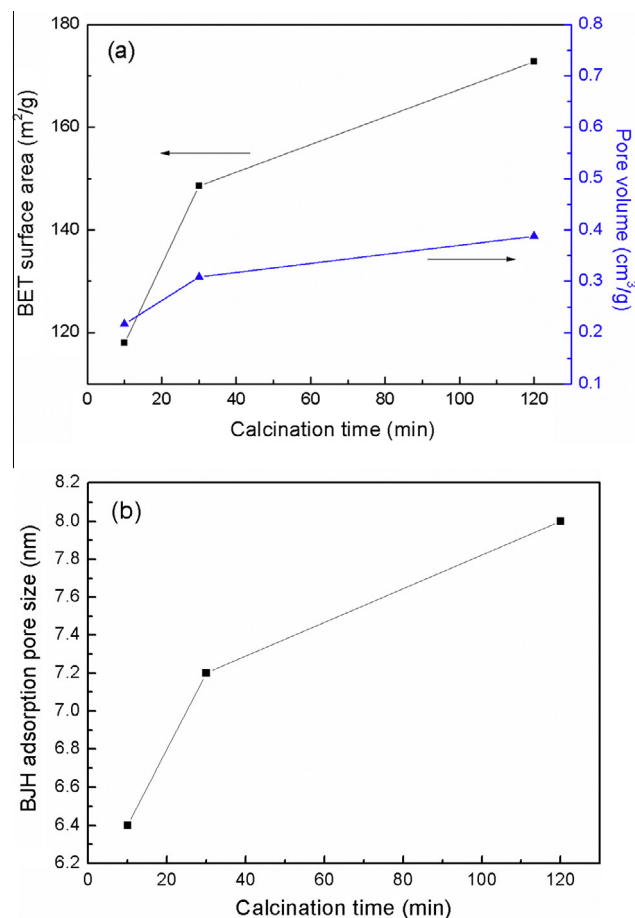


Fig. 6. The TiO₂ precursor powder with residual NH₄Cl content was calcining at 573 K for various times: (a) BET specific surface area and pore volumes, and (b) BJH average pore size.

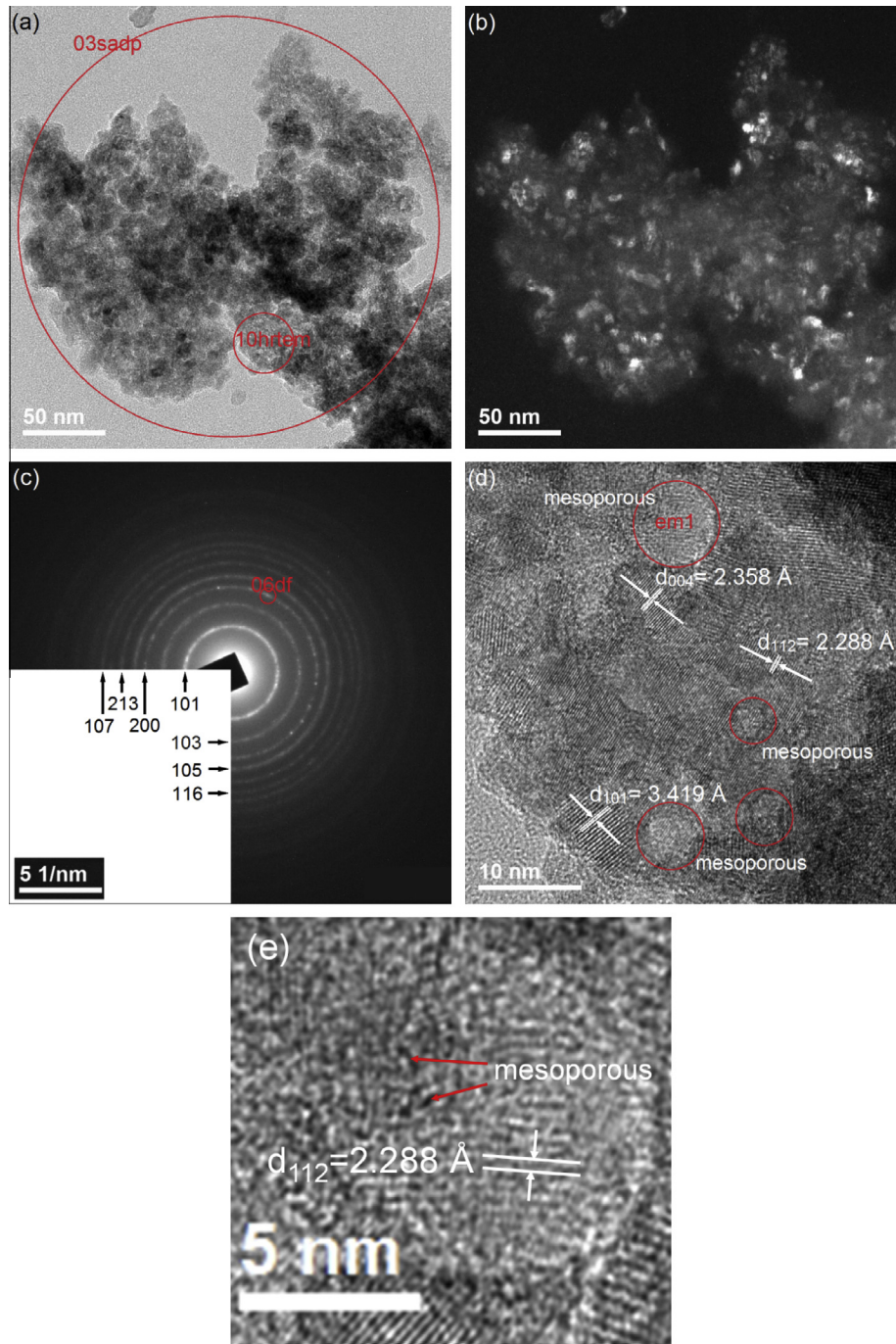


Fig. 7. TEM micrographs, SAED pattern and HRTEM image of TiO_2 precursor powder with residual NH_4Cl content calcined at 573 K for 1 h: (a) BF image, (b) DF image of the circle denoted by 06df in (c), (c) SAED pattern of the location area denoted by 03sadb in (a), which is indexed as corresponding to anatase TiO_2 , and (d) HRTEM of the location area denoted by 10hrtem in (a), shows the d -spacings of anatase TiO_2 (101), (004) and (112) reflections are 3.419, 2.358 and 2.288 Å, respectively, and indicates the mesoporous structure by arrows, and (e) an enlarged view of location area denoted by em1 in (d), which shows that the d -spacing of anatase TiO_2 (112) is 2.288 Å and indicates the mesoporous structure by arrows.

BET surface area underwent a large increase as the calcination temperature rose from 473 to 573 K. This happened because although the anatase TiO_2 crystallite size only increased from 3.3 to 6.5 nm and accompanied the small amount of type II NH_4Cl that appeared. However, the type I NH_4Cl completely decomposed and created the surface area increased becomes so accelerated.

The BET surface area decreased rapidly from 172.8 to 95.8 m^2/g when the calcination temperature rose from 573 to 673 K. The crystallite size of anatase TiO_2 was 10.5 nm and the crystallinity also increased after the precursor powder was calcined at 673 K

for 2 h. Therefore, the BET surface area decreased due to the crystallization of anatase TiO_2 , subsequent crystallite growth, and the collapse of the mesoporous structure [33,34].

The pore volumes of mesoporous anatase TiO_2 powers obtained by the BET method are also listed in Table 2. It can be seen that the values for pore volume increased with increasing calcination temperature. The pore volume in the mesoporous TiO_2 powder was mainly affected by TiO_2 crystallite growth [29], i.e. influenced by calcination temperature. For the TiO_2 precursor powder with residual NH_4Cl content after calcining at 473 K for 2 h, the anchoring of

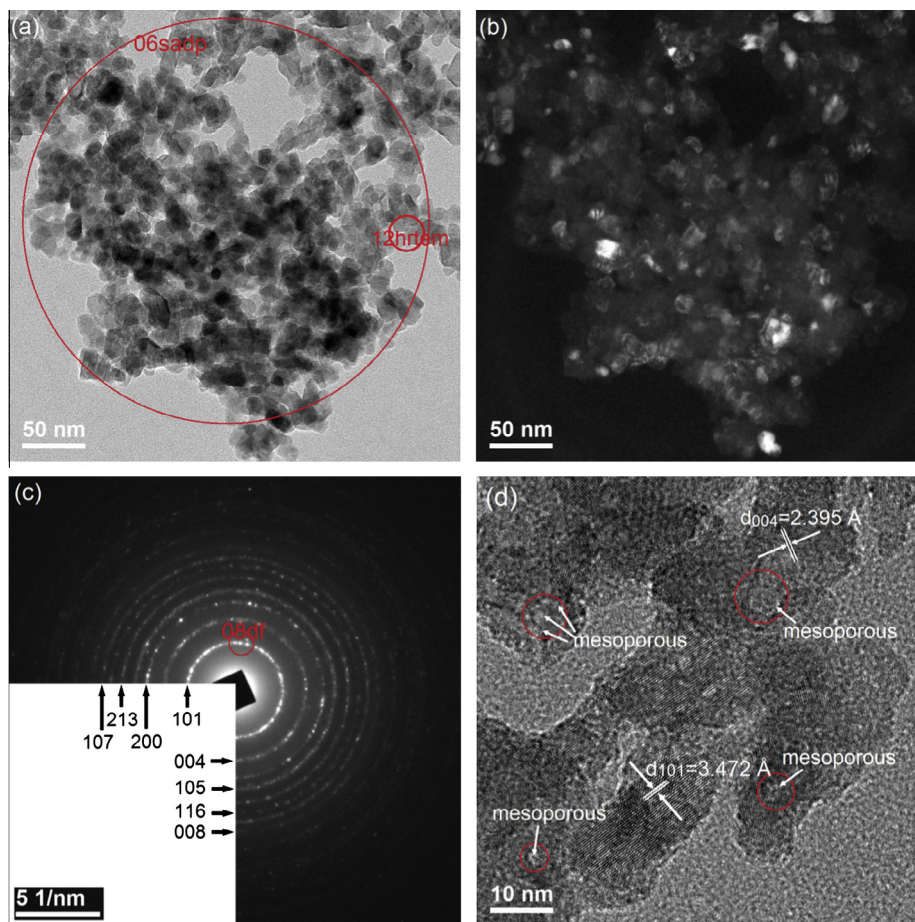


Fig. 8. TEM micrographs, SAED pattern and HRTEM image of TiO_2 precursor powder with residual NH_4Cl content calcined at 673 K for 2 h: (a) BF image, (b) DF image of the circle denoted by 08df in (c), (c) SAED pattern of the location area denoted by 06sadb in (a), which is indexed as corresponding to anatase TiO_2 , and (d) HRTEM of the location area denoted by 12hrtem in (a), shows the d -spacings of the anatase TiO_2 (101) and (004) reflections are 3.472 and 2.395 Å, respectively, and indicates the mesoporous structure by arrows.

type I NH_4Cl in the framework of the calcination product efficiently restrained the growth of anatase TiO_2 crystallites. Therefore, the calcination product only had a very smaller pore volume of $0.081 \text{ cm}^3/\text{g}$. Nevertheless, when the calcination temperature rose from 473 to 573 K, the decomposition of type I NH_4Cl was completed and accompanied by a minor phase of type II NH_4Cl formation, creating the accelerated increase in pore volume. When the TiO_2 precursor powder was calcined at 673 K for 2 h, the pore volume was only slightly increased. This result is attributed to the anatase crystallite growth from 6.5 to 10.5 nm and only a minor amount of decomposition of type II NH_4Cl .

However, Kim et al. [34] synthesized monodisperse spherical mesoporous TiO_2 particles with controlled size by a simple sol-gel method and pointed out that the pore volume decreased with increasing calcination temperature. This result is not in agreement with the present study.

The average pore size of TiO_2 precursor powder with residual NH_4Cl after calcining at various temperatures for 2 h was determined by the BJH method [35] and the results are shown in Fig. 5. The BJH adsorption pore sizes obtained are also listed in Table 2. In fact, Fig. 5(a) shows that TiO_2 precursor powder has a narrower pore size distribution after calcining at 473 K compared to calcining at other temperatures with an evident peak at 2.57 nm. In addition, the pore size distribution also revealed that TiO_2 precursor powder calcination at 573 K yielded a smaller pore size (8.0 nm) than at 673 K (14.0 nm). According to the results in Fig. 4, the observed hysteresis loops shifts to a higher relative pressure of $P/P_0 = 1$ can be suggesting the large

pores appeared when calcined at 673 K [9]. A bimodal pore size distribution was observed for calcination at 473 K. This result was due to uncontrollable pore collapse during the calcination stage [6].

The average pore size increases with increasing anatase TiO_2 crystallite size, as confirmed by the XRD analysis (see Table 1), and the pore size distribution also becomes broader with rising calcination temperature, revealing that the pores from the decomposition of type I and type II NH_4Cl have many pores. This result is not in agreement with the pores formed from the assembly of TiO_2 nanoparticles [36].

The dependence of BET specific surface area and pore volume of TiO_2 precursor powder after calcining at 573 K for various times are shown in Fig. 6(a). It can be seen that the specific surface area and pore volume increase from 118.2 to $172.8 \text{ m}^2/\text{g}$ and 0.217 to $0.388 \text{ cm}^3/\text{g}$, respectively, as the calcination time increased from 10 to 120 min. These results were attributed to a slight increase in the decomposition of type II NH_4Cl with increasing calcination time. In addition, the crystallite size of anatase TiO_2 gradually grew, also influencing the specific surface area and pore volume and leading to their increases.

Fig. 6(b) shows the BJH adsorption pore size distribution of TiO_2 precursor powder after calcining at 573 K for several different periods of time. It reveals that the average pore size of mesoporous anatase TiO_2 powder increased from 6.4 to 8.0 nm with increasing the duration at 573 K. In fact, the factors influencing the average pore size were similar to those affecting the specific surface area and pore volume of anatase TiO_2 mesoporous powders.

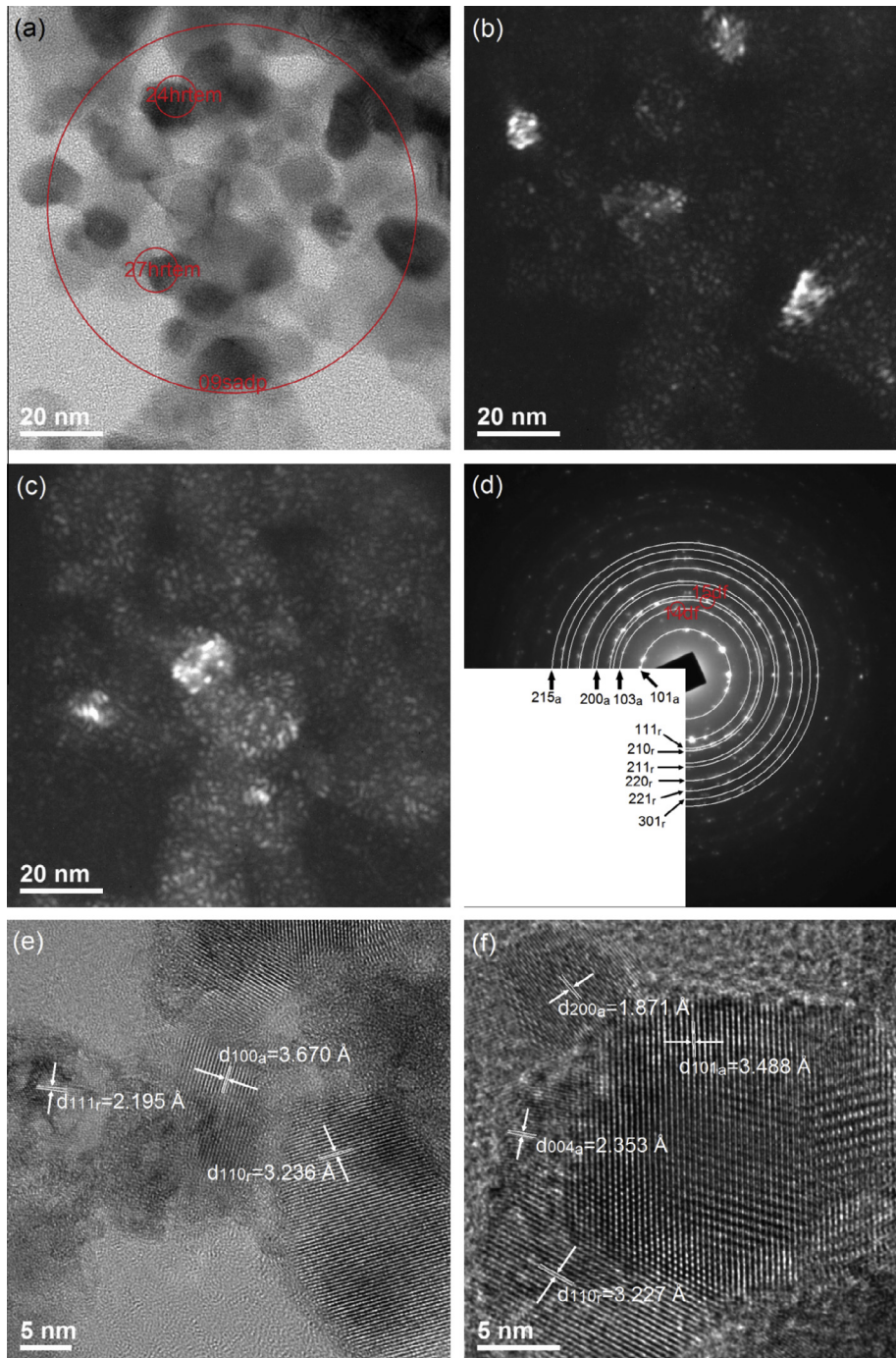


Fig. 9. TEM micrographs, SAED pattern and HRTEM image of TiO_2 precursor powder with residual NH_4Cl content calcined at 773 K for 2 h: (a) BF image, (b) and (c) are DF images using the circle denoted by 14df and 15df in (d), respectively, (d) SAED pattern of the location area denoted by 09sadb in (a), which is indexed as corresponding to coexisting phases of anatase and rutile TiO_2 , (e) and (f) are HRTEM images of the location area denoted by 24hrtem and 27hrtem in (a), respectively. (e) Shows the d -spacing of the anatase TiO_2 (100) reflection is 3.670 Å, and those of the rutile TiO_2 (110) and (111) reflections are 3.236 and 2.195 Å, respectively. (f) Shows the d -spacings of anatase TiO_2 (101), (004) and (200) reflections are 3.488, 2.353 and 1.871 Å, respectively, and that of the rutile TiO_2 (110) reflection is 3.227 Å.

As mentioned above, using residual NH_4Cl in the TiO_2 precursor powder and calcining at 673 K for 2 h, a single phase of anatase TiO_2 mesoporous powder with suitable pore size was obtained and the residual NH_4Cl was fully removed. Therefore, a single phase of anatase TiO_2 mesoporous powder was successfully obtained by an in situ synthesis using a coprecipitation process.

Fig. 7 shows TEM bright field (BF), dark field (DF) micrographs, SAED pattern and high resolution TEM (HRTEM) images of TiO_2 precursor powder with residual NH_4Cl content calcined at 573 K for 1 h. Fig. 7(a) illustrates the BF micrograph, which indicates that

many particles had been incorporated and were difficult to resolve given their small size. This result was due to the TiO_2 precursor powder being synthesized using the coprecipitation method, during which, after drying and/or subsequent processing, agglomeration can occur [37]. A DF micrograph of the calcined powder using the circle denoted by 06df in Fig. 7(c) is shown in Fig. 7(b). It is seen that the nanopowder was crystallized and the crystallite size was about 6.0 ± 1.7 nm. Fig. 7(c) shows the SAED pattern of the location area denoted by 03sadb in Fig. 7(a), which shows the (101), (103), (200), (105), (213), (116) and (107) reflections of

anatase TiO₂. The Debye rings reveal that the calcined powder was polycrystalline. The diffraction rings in the SAED pattern correspond well to the XRD reflection peaks. Fig. 7(d) shows the HRTEM image of the location area denoted by 10hrtem in Fig. 7(a). It can be seen that the mesopores in Fig. 7(d) denoted by circle. In addition, the HRTEM image also shows *d*-spacings of 3.419, 2.288 and 2.358 Å for the anatase TiO₂ (101), (112) and (104) reflection planes, respectively. Fig. 7(e) shows an enlarged view of location area denoted by em1 in Fig. 7(d). It reveals that the *d*-spacing of anatase TiO₂ (112) is 2.288 Å. On the other hand, Fig. 7(e) also indicates that the mesoporous size is about 1.0–2.0 nm.

TEM BF and DF micrographs, SAED pattern and HRTEM images of the TiO₂ precursor powder with residual NH₄Cl content calcined at 673 K for 2 h are shown in Fig. 8. Fig. 8(a) shows a BF micrograph of the calcined powder, which reveals that the crystallites were still agglomerated so it is too difficult to discriminate individual crystallites. However, the crystallinity of the crystallites continuously improved as the calcination temperature increased. Fig. 8(b) shows a DF image of the calcined product in the circle denoted by 08df in Fig. 8(c), which reveals the crystalline size to be about 12.5 ± 2.5 nm. The SAED pattern of the location area denoted by 03sadb in Fig. 8(a) is shown in Fig. 8(c), which is indexed as corresponding to anatase TiO₂. The SAED pattern also provides that after the precursor powder was calcined at 673 K for 2 h the anatase TiO₂ was still maintained. Fig. 8(d) shows a HRTEM image of the location area denoted by 12hrtem in Fig. 8(a). It shows the mesoporous structure in the anatase TiO₂ crystallites as denoted by circles and indicated by arrows. In addition, the HRTEM image also reveals that the calcined product exhibited clear lattice fringes. The HRTEM image also shows that the *d*-spacings of anatase TiO₂ (101) and (004) are 3.472 and 2.395 Å, respectively.

Fig. 9 shows the TEM BF and DF micrographs, an SAED pattern and HRTEM image of the TiO₂ precursor powder with residual NH₄Cl content calcined at 773 K for 2 h. Fig. 9(a) shows the BF image, which reveals that fine crystallites were gradually incorporated into larger particles with rising calcination temperature. Fig. 9(b) and (c) shows DF micrographs of the calcined product using the circle denoted by 14df and 15df in Fig. 9(d). Fig. 9(d) shows the SAED pattern of location area denoted by 09sadb in Fig. 9(a), revealing the (101), (103), (200) and (215) reflections from anatase TiO₂. Moreover, Fig. 9(d) also shows the (111), (210), (211), (220), (221) and (301) reflections from the rutile TiO₂. Fig. 9(d) also provides an evidence for a phase transition from anatase to rutile TiO₂ occurred when the TiO₂ precursor powder was calcined at 773 K for 2 h. From the indexed result in Fig. 9(d), it is also apparent that Fig. 9(b) and (c) show crystallites of anatase and rutile TiO₂, respectively. Fig. 9(e) and (f) shows HRTEM images of location area denoted by 27hrtem and 24hrtem, respectively, in Fig. 9(a). They reveal that the calcined product exhibited good crystallinity, clear lattice fringes and was mesoporous. Fig. 9(e) shows that the *d*-spacing of the anatase TiO₂ (100) is 3.670 Å, and rutile TiO₂ (110) and (111) are 3.236 and 2.195 Å, respectively. On the other hand, Fig. 9(f) also shows that the *d*-spacings of the anatase TiO₂ (101), (004) and (200) reflections are 3.488, 2.353 and 1.871 Å, respectively, and the rutile TiO₂ (110) reflection is 3.227 Å.

4. Conclusions

The characteristics and properties of TiO₂ precursor powder with residual NH₄Cl content after calcining were investigated using DSC/TG, XRD, BET and BJH analyses, TEM, SAED and HRTEM. The results of the present study can be summarized as follows:

- (1) The TiO₂ precursor powder contained anatase and 19.5% NH₄Cl.

- (2) Before calcining the precursor powder contained type I NH₄Cl and anatase TiO₂ as the primary and secondary phases, respectively. When calcined at 573 K for 2 h, phases of anatase TiO₂ and type II NH₄Cl coexisted in the calcined product. However, the calcined product only contained a single phase of anatase TiO₂ when the precursor powder was calcined at 673 K for 2 h. Moreover, anatase and rutile coexist as the primary and secondary phases in the calcined products.
- (3) The crystallite size of anatase increased from 3.3 to 14.3 nm when the precursor powder calcination temperature was increased from 473 to 773 K. In addition, the crystallite size of rutile TiO₂ was 26.6 nm when the precursor powder was calcined at 773 K for 2 h.
- (4) When the TiO₂ precursor powder with residual NH₄Cl content was calcined at 673 K for 2 h, the BET specific surface area was affected. The maximum value of the BET specific surface area and pore volume were 172.8 m²/g and 0.392 cm³/g, respectively. When the powder was at various temperatures for 2 h, the average pore size increased from 3.80 to 14.0 nm as the calcination temperature rose from 473 to 773 K.
- (5) Mesoporous anatase TiO₂ nanopowders were successfully synthesized when the TiO₂ precursor powder with residual NH₄Cl content and without an added surfactant agent was calcined at 673 K for 2 h.

Acknowledgements

The authors sincerely thank the National Science Council of Taiwan for its financial support under NSC 100-2221-E-037-001. The authors also gratefully acknowledge the help of Mr. S.Y. Yao for TEM.

References

- [1] D. Fairhurst, M.A. Mitchnick, in: N.J. Lowe, N.A. Shaath, M.A. Pathak (Eds.), *Sunscreen-Development, Evaluation and Regulation Aspects*, second ed., Marcel Dekker, New York, 1997, pp. 313–352.
- [2] T.G. Smijs, S. Pavel, Titanium dioxide and zinc oxide nanoparticles in sunscreens: focus on their safety and effectiveness, *Nanotechnol. Sci. Appl.* 4 (2011) 95–112.
- [3] D.A.H. Hanaor, C.C. Sorrell, Review of the anatase to rutile phase transformation, *J. Mater. Sci.* 46 (2011) 855–874.
- [4] M. Grujić-Brojčin, S. Armaković, N. Tomić, B. Abramović, A. Golubović, B. Stojadinović, A. Kremenović, B. Babić, Z. Dohčević-Mitrović, M. Šćepanović, Surface modification of sol-gel synthesized TiO₂ nanoparticles induced by L-doping, *Mater. Charact.* 88 (2014) 30–41.
- [5] M. Šćepanović, B. Abramović, A. Golubović, S. Kler, M. Grujić-Brojčin, Z. Dohčević-Mitrović, B. Babić, B. Matović, Z.V. Popović, Photocatalytic degradation of metoprolol in water suspension of TiO₂ nanopowders prepared using sol-gel route, *J. Sol-Gel Sci. Technol.* 61 (2012) 390–422.
- [6] K.H. Leong, P. Monash, S. Ibrahim, P. Saravanan, Solar photocatalytic activity of anatase TiO₂ nanoparticles synthesized by non-hydrolytic sol-gel method, *Sol. Energy* 101 (2014) 321–332.
- [7] J. Yang, S. Mei, J.M.F. Ferreira, Hydrothermal synthesis of nanosized titania powders: influence of tetraalkyl ammonium hydroxides on particle characteristic, *J. Am. Ceram. Soc.* 84 (2001) 1696–1702.
- [8] S.-I. Kawasaki, Y. Xiuyi, K. Sue, Y. Hakuta, A. Suzuki, K. Arai, Continuous supercritical hydrothermal synthesis of controlled size and highly crystalline anatase TiO₂ nanoparticles, *J. Supercrit. Fluids* 50 (2009) 276–282.
- [9] H. Tang, D. Zhang, G. Tang, X. Ji, W. Li, C. Li, X. Yang, Hydrothermal synthesis and visible-light photocatalytic activity of α-Fe₂O₃/TiO₂ composite hollow microspheres, *Ceram. Int.* 39 (2013) 8633–8640.
- [10] S.W. Yeh, Y.L. Chen, C.S. Hsi, H.H. Ko, M.C. Wang, Thermal behavior and phase transformation of TiO₂ nanocrystallites prepared by a coprecipitation route, *Metall. Mater. Trans. A* 45A (2014) 261–268.
- [11] H.H. Ko, C.S. Hsi, M.C. Wang, X. Zhao, Crystallite growth kinetic of TiO₂ surface modified with 9 mol% ZnO prepared by a coprecipitation process, *J. Alloys Comp.* 588 (2014) 428–439.
- [12] D.M. Antonelli, J.Y. Ying, Synthesis of hexagonally-packed mesoporous TiO₂ by a modified sol-gel method, *Angew. Chem. Int. Ed. Engl.* 34 (1995) 2014–2017.
- [13] I.M. Hung, Y. Wang, C.F. Huang, Y.S. Fan, Y.J. Han, H.W. Peng, Effect of templating surfactant concentrations on the mesostructure of ordered

- mesoporous anatase TiO₂ by an evaporation-induced self-assembly method, *J. Eur. Ceram. Soc.* 30 (2010) 2065–2072.
- [14] D.S. Kim, S.J. Han, S.Y. Kwak, Synthesis and photocatalytic activity of mesoporous TiO₂ with the surface area, crystallite size and pore size, *J. Colloid Interface Sci.* 316 (2007) 85–91.
- [15] S.J.F. Herregods, M. Mertens, K.V. Havenbergh, G.V. Tendeloo, P. Cool, A. Buekenhoudt, V. Meynen, Controlling pore size and uniformity of mesoporous titania by early stage low temperature stabilization, *J. Colloid Interface Sci.* 391 (2013) 36–44.
- [16] S. Casino, F. Di Lupo, C. Francia, A. Tuel, S. Bodoardo, C. Gerbaldi, Surfactant-assisted sol gel preparation of high-surface area mesoporous TiO₂ nanocrystalline Li-ion battery anodes, *J. Alloys Comp.* 594 (2014) 114–121.
- [17] B.D. Cullity, *Element of X-ray Diffraction*, Addison-Wesley, Reading (MA), 1967, p. 170.
- [18] R.A. Spurr, H. Myers, Quantitative analysis of anatase-rutile mixture with an X-ray diffractometer, *Anal. Chem. Res.* 29 (1957) 760–762.
- [19] Y.W. Hsu, K.H. Yang, K.M. Chang, S.W. Yeh, M.C. Wang, Synthesis and crystallization behavior of 3 mol% yttria stabilized tetragonal zirconia polycrystals (3Y-TZP) nanosized powders prepared using a simple coprecipitation process, *J. Alloys Comp.* 509 (2011) 6864–6870.
- [20] G. Li, L. Li, J. Boerio-Goates, B.F. Woodfield, High purity anatase TiO₂ nanocrystals: near room-temperature synthesis, grain growth kinetics and surface hydrogen chemistry, *J. Am. Chem. Soc.* 127 (2005) 8659–8666.
- [21] M. Henry, J.P. Jolivet, J. Livage, *Aqueous Chemistry of Metal Cations, Hydrolysis, Condensation and Complexation*, Springer, Berlin, 1992, p. 155.
- [22] S.T. Aruna, S. Tirosh, A. Zaban, Nanosize rutile titania particle synthesis via a hydrothermal method, *J. Mater. Chem.* 10 (2000) 2388–2391.
- [23] D. Zhang, L. Qi, J. Ma, H. Chang, Formation of crystalline nanosized titania in reverse micelles at room temperature, *J. Mater. Chem.* 12 (2002) 3677–3680.
- [24] H.S. Liu, T.S. Chin, S.Y. Chiu, K.H. Chung, C.S. Chung, M.T. Liu, Hydroxyapatite synthesized by a simplified hydrothermal method, *Ceram. Int.* 23 (1997) 19–25.
- [25] C.W. Kuo, Y.H. Shen, S.B. Wen, H.E. Lee, I.M. Hung, H.H. Huang, M.C. Wang, Phase transformation kinetics of 3 mol% yttria partially stabilized zirconia (3Y-TZP) nanopowders prepared by a non-isothermal process, *Ceram. Int.* 37 (2011) 341–347.
- [26] C.C. Wang, J.Y. Ying, Sol-gel synthesis and hydrothermal processing of anatase and rutile titania nanocrystals, *Chem. Mater.* 13 (1999) 3113–3120.
- [27] X.M. He, Q.L. Xie, J. Liu, W.G. Lan, H.P. Xia, Photocatalytic activity of size and phase selective TiO₂ photocatalyst nanoparticles prepared by the membrane processing, *Sep. Purif. Technol.* 68 (2009) 153–158.
- [28] A.R. Liu, S.M. Wang, Y.R. Zhao, Z. Zheng, Low-temperature preparation of nanocrystalline TiO₂ photocatalyst with a very large specific surface area, *Mater. Chem. Phys.* 99 (2006) 131–134.
- [29] X.M. Yan, P. Mei, J. Lei, Y. Mi, L. Xiong, L. Guo, Synthesis and characterization of mesoporous phosphotungstic acid/TiO₂ nanocomposite as a novel oxidative desulfurization catalyst, *J. Mol. Catal. A: Chem.* 304 (2009) 52–57.
- [30] M. Kruk, M. Jaroniec, Gas adsorption characterization of ordered organic-inorganic nanocomposite materials, *Chem. Mater.* 13 (2001) 3169–3183.
- [31] F. Dumeignil, K. Sato, M. Imamura, N. Matsubayashi, E. Payen, H. Shimada, Modification of structural and acidic properties of sol-gel prepared alumina powders by changing the hydrolysis ratio, *Appl. Catal., A* 241 (2003) 319–329.
- [32] C. Li, Y. Luo, X. Guo, D. Li, J. Mi, L. Sφ, P. Hald, Q. Meng, B.B. Iversen, Mesoporous TiO₂ aggregate photoanode with high specific surface area and strong light scattering for dye-sensitized solar cells, *J. Solid State Chem.* 196 (2012) 504–510.
- [33] D.C.M. Dutoit, Synthesis of phosphorus-free mesoporous titania via templating with amine surfactants, *Microporous Mesoporous Mater.* 30 (1999) 315–319.
- [34] D.S. Kim, J.D. Joen, K.H. Shin, The size controlled synthesis of monodisperse spherical mesoporous TiO₂ particles and high dispersions of Pt, Pd and Ag clusters on their surfaces, *Microporous Mesoporous Mater.* 181 (2013) 61–67.
- [35] E.P. Barrett, L.G. Joyner, P.P. Halenda, The determination of pore volume and area distribution in porous substances. I. Computations from nitrogen isotherms, *J. Am. Chem. Soc.* 73 (1951) 373–380.
- [36] T.Z. Ren, Z.Y. Yuan, B.L. Su, Surfactant-assisted preparation of hollow microspheres of mesoporous TiO₂, *Chem. Phys. Lett.* 374 (2003) 170–175.
- [37] M.C. Wang, The effect of TiO₂ on the preparation and phase transformation for precursor β-spodumene powders, *J. Mater. Res.* 8 (1994) 2290–2297.